Observation of collapsing radiative shocks in laboratory experiments

A. B. Reighard, R. P. Drake, K. K. Dannenberg, D. J. Kremer, M. Grosskopf, E. C. Harding, and D. R. Leibrandt
Department of Atmospheric Oceanic and Space Sciences, University of Michigan, Ann Arbor, Michigan 48109

S. G. Glendinning, T. S. Perry, B. A. Remington, and J. Greenough
Lawrence Livermore National Laboratory, Livermore, California 94551

J. Knauer and T. Boehly
Laboratory for Laser Energetics, University of Rochester, Rochester, New York 14623

S. Bouquet
Département de Physique Théorique et Appliquée (DPTA), CEA-DIF, BP 12, 91680 Bruyères-le-Châtel, France

L. Boireau
Département de Physique Théorique et Appliquée (DPTA), CEA-DIF, BP 12, 91680 Bruyères-le-Châtel, France, and LUTH, Observatoire de Paris, Paris, France

M. Koenig and T. Vinci
Laboratoire pour l'Utilisation des Lasers Intenses, Ecole Polytechnique, 91128 Palaiseau, France

(Received 27 March 2006; accepted 21 June 2006; published online 3 August 2006)

This article reports the observation of the dense, collapsed layer produced by a radiative shock in a laboratory experiment. The experiment uses laser irradiation to accelerate a thin layer of solid-density material to above 100 km/s, the first to probe such high velocities in a radiative shock. The layer in turn drives a shock wave through a cylindrical volume of Xe gas (at ~ 6 mg/cm^3). Radiation from the shocked Xe removes enough energy that the shocked layer increases in density and collapses spatially. This type of system is relevant to a number of astrophysical contexts, providing the potential to observe phenomena of interest to astrophysics and to test astrophysical computer codes. © *2006 American Institute of Physics*. [DOI: 10.1063/1.2222294]

I. INTRODUCTION

Radiative shocks are a type of radiative hydrodynamic phenomenon. Shock waves heat the material they pass through, and first become radiative shocks when the radiative flux from the hot material becomes energetically significant. Radiative shocks abound in the universe, but their study in the laboratory is relatively new. Creation of these systems requires temperatures of tens of electron volts or more, sufficient to create ionized matter in which at minimum radiative energy fluxes locally can exceed material energy fluxes. In any radiative shock there is an "optically thin" region (having small optical depth) where radiative effects are large, near the density jump. Here by "optical depth" we refer to the number of e-foldings of attenuation of thermal radiation. The optical depth of the entire system on each side of the density jump corresponding to the shock determines the detailed properties of radiative shocks,[1,2] including the extent of the region over which radiative effects are large. In experiments on radiative shocks, the optical depth, for the thermal radiation from the shocked matter, must be adequate to allow significant energy exchange between matter and radiation on the time scale of the experiment. There is also in principle a regime of very high temperature and very large optical depth in which the radiation pressure can exceed the material pressure.[1] Current experiments cannot reach this regime but can reach the regime of large radiative fluxes just described.

Achieving both high enough temperature and sufficient optical depth simultaneously requires the use of high-energy-density facilities. Little laboratory data exist on radiative shocks, as they are difficult to establish under controlled conditions. If the region on either side of the shock is "optically thin" (easily allows the passage of the thermal radiation from the shocked matter), the density of the shocked layer can increase greatly as it cools by radiating away its energy.[3,4] The thickness of the shocked layer correspondingly decreases, so the shock can be said to collapse. Here we report a laboratory experiment to observe, for the first time, the collapsed layer produced by a radiative shock.

Radiation and radiative collapse both play important roles in astrophysical shock waves. The shock wave emerging from a supernova passes through a regime in which the shocked layer collapses in space because of radiative energy losses.[5] Similar dynamics can occur at the accretion shocks produced during star formation,[6–8] and at the reverse shock in a supernova remnant formed from a star with a dense stellar wind[9] or preexisting dense material as in supernova 1987A.[10,11] Stratified ionization states form in a radiative precursor of a Herbig-Haro object with a radiative cooling layer.[12] There is more generally a radiative cooling zone behind most astrophysical shocks. Collapse of an existing shocked layer can occur in some cases, as, e.g., in aging

supernova remnants in which the shocked layer is no longer driven.[13]

One can organize the prior laboratory work on radiating shock waves by the strength of the radiative effects that were present, which scale very strongly with shock velocity, u_s. Experiments discussed by Edwards *et al.*[14] produced $u_s \sim 8$ km/s in a cylindrical blast wave, and observed radiative cooling effects that resulted from heating of the shocked gas by electron heat conduction. At higher u_s, experiments can exceed the threshold[15] for the formation of a thermal radiative precursor, in which thermal radiation from matter heated by the shock itself heats the matter ahead of ("upstream" of) the shock. Radiative precursors have been observed in experiments by Bozier *et al.*,[16] Grun *et al.*,[17] Keiter *et al.*,[15] Bouquet *et al.*,[18] Koenig *et al.*,[19,20] and Vinci.[21] The experiment of Grun *et al.*[17] produced a quasispherical radiative blast wave, in which radiation during the shock transition is calculated to play a key role.[22]

The present experiment is the first in planar geometry to exceed the threshold for radiative collapse by formation of a postshock cooling layer, and to detect the material that has been shocked and cooled. Following the shock, which heats ions primarily, the ions and electrons equilibrate rapidly compared to the rate of radiative cooling. The resulting, initial postshock electron and ion temperature for a strong shock, T_{init}, is[4]

$$T_{\text{init}} = \frac{2}{(\gamma+1)^2}\frac{u_s^2}{c_v}, \tag{1}$$

in which γ is the polytropic index appropriate to the shock transition and c_v is the specific heat at constant volume of the postshock material, equal to $3(Z+1)k_B/(2Am_p)$ for a fully ionized gas. (Here k_B is the Boltzmann constant, m_p is the proton mass, and Z and A are the average ionization and atomic mass numbers, respectively.) In a material like xenon, c_v and γ both should include the effects of ionization. A postshock cooling layer must form when the energy flux due to thermal radiative losses from the shocked material exceeds the energy flux entering the shocked material. This natural normalization of the fluid energy equation in an optically thick system gives a threshold for significant radiative cooling as $R_r > 1$, where

$$R_r = \frac{(\gamma+1)}{\gamma}\frac{4\sigma T_{\text{init}}^4}{\rho_0 u_s^3} = \frac{64}{\gamma(\gamma+1)^7}\frac{\sigma}{c_v^4}\frac{u_s^5}{\rho_0}, \tag{2}$$

in which σ is the Stefan-Boltzmann constant and ρ_0 is the mass density of the unshocked, upstream material. The corresponding threshold velocity[23] in xenon, at 10 mg/cm^3, is approximately 50 km/s. If the optical depth of the region behind the shock decreases, decreasing the emissivity of the shocked material, the value of R_r required to see large radiative effects increases.

II. EXPERIMENT

We drive a planar, radiative shock through a xenon-filled target and observe the structure of the shocked xenon layer. Figure 1 shows a target schematic. The inside diameter (i.d.) of the gas cell was either 600 or 912 μm. We used the fill tube to evacuate the target and then fill it with xenon. The xenon pressure was measured for each experiment, and was 1.1 ($\pm 10\%$) atm for the cases of interest here corresponding to $\rho_0 = 6$ mg/cm^3 or to 2.7×10^{19} atoms/cm^3. The drive disk was either 51 μm of polyimide ($\pm 3\%$ and at 1.41 g/cm^3) overcoated with 20 ($+5/-10$) μm of polyvinyl at 1 g/cm^3, or 20 μm or 40 μm ($\pm 7\%$) of Be. We focused ten laser beams of wavelength 0.35 μm onto a 1 mm spot centered on the ~ 2.5 mm diameter drive disk in a square, 1 ns flat-top pulse, with the midpoint of the rising edge defining time $t=0$. The total energy was $\leqslant 4000$ J. Distributed phase plates (DPPs) created super-Gaussian focal spots of 720 or 820 μm diameter (full width at half-maximum), with small-scale structure which fluctuated via smoothing by spectral dispersion (SSD). The resulting laser irradiance was up to 10^{15} W/cm^2. The pressure from laser ablation first shocked and then accelerated the drive disk, launching it into the xenon and driving a shock.

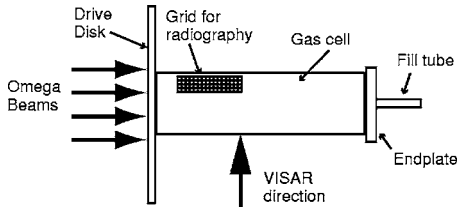

FIG. 1. Target diagram. In this view the backlighter plate would sit directly behind target, below the plane.. When the VISAR (velocity interferometer system for any reflector) diagnostic was used (see the text for reference), additional arms were added to hold a quartz window and a mirror for the VISAR laser, and shielding was added behind the drive disk and to the left of the arms to reduce preheating of the gas in the arms. When a point backlighter was used, its line of sight was in the same direction as the VISAR line of sight.

X-ray radiography was the principal diagnostic, using two types of x-ray sources called "backlighters." The laser beams producing the x rays were of the same wavelength and laser pulse as given previously, at a nominal energy of 450 J/beam, without SSD and usually without DPPs. Some shots included an "area backlighter," in which such laser beams were focused to a ~ 1 mm spot on a vanadium foil several square millimeters in area and 5 μm thick, to produce K-shell emission at ~ 5.2 keV. This millimeter-sized source was placed 4 ± 0.25 mm from the target, and imaged onto a framing camera[24] through pinholes. A "backlit pinhole" was also used on some shots, where the laser beams were focused to a 400 μm spot on a 5 μm thick V foil, spaced by 100 μm of CH behind an 80 μm thick Ta substrate with a 20 μm through hole, covered by 100 μm of CH. This small x-ray source was located 12 ± 0.1 mm from the target, and projected a radiograph of the target onto a framing camera located ~ 229 mm beyond it. Due to vignetting, the effective source size for this measurement was ~ 15 μm. A gold grid was placed on the target to calibrate the location and magnification of the image. A velocity interferometer system for any reflector (VISAR) diagnostic (see Fig. 1) was also used in some cases.

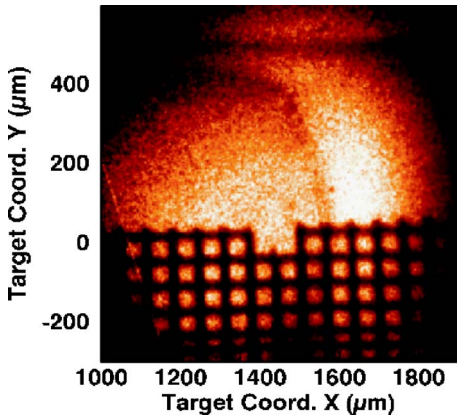

FIG. 2. (Color online) Radiography image from an area backlighter, at 13.5 ns, from an experiment with a polyimide drive disk attached to a polyimide tube of 912 μm i.d., irradiated with SSD at 9.3×10^{14} W/cm^2 onto a 720 μm laser spot. The illumination was by x rays from V produced by overlapping six laser beams. The grid with a fiducial feature establishing an absolute location is evident in the lower part of the figure. The wall of the tube can be seen near the upper edge.

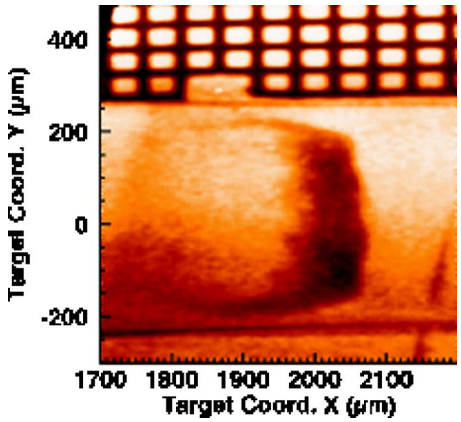

FIG. 3. (Color online) Radiography image from a point-projection backlighter, or a "backlit pinhole," from an experiment with a 20 μm drive disk attached to a polyimide tube of 575 μm i.d., irradiated with SSD at 4.8×10^{14} W/cm^2 onto an 820 μm laser spot, again using a V backlighter. The same type of fixed spatial fiducial is present, as are the tube walls. The shock is tilted in the plane of the image, but some evidence of trailing xenon along the tube walls is present.

III. EXPERIMENTAL RESULTS

Radiography of the shock in xenon shows clear indications of a thin, dense shock. On a range of experiments, we have seen dense shocked layers with thicknesses ranging between 45 and 80 μm. In the plane of the radiograph, some layers were tilted with respect to the target axis by as much as 10°. We show the thinnest of these layers in Fig. 2, taken at 13.5±0.3 ns, with the region of highest opacity being 45 μm thick. One can see the center of the shock (which is moving to the right) at approximately 1600 μm from the initial driven surface, with indications of a trailing layer of dense xenon along the wall of the tube. The velocity averaged over the first 13.5 ns is 118 km/s. Figure 3 shows a typical radiograph with a thicker layer, from an experiment with a 22 μm drive disk and a 10% lower drive irradiance. In this image, the center of the layer has moved 1150 μm in 8.0±0.3 ns, where its thickness is 65 μm. The average velocity of the shock until this time is ~140 km/s.

When the VISAR diagnostic was used,[25] fringe patterns from the VISAR diagnostic ceased before the drive laser shut off. We attribute this to collisional absorption in the Xe gas, heated to a few eV by radiative preheat.[26] Later, a thin feature appeared, showing no fringes and nonuniform in space and duration. We attribute this signal to reflection of the interferometer beam from the edge of the shock front. The shock velocity inferred from this is consistent with that determined from the radiographic data.

Even without any input from computer simulations, the data provide strong evidence that there is a shock that has significantly collapsed. Assuming that two-dimensional (2D) lateral flow is small, which is supported by the limited layer of absorbing material along the tube wall in the image and also by the simulations discussed below, the thickness of the layer corresponds directly to the amount of compression in the shock. For the thinnest observed thickness of 45 μm, assuming the line of sight to be exactly side on and given the instrumental resolution of 10 μm, one concludes that the data image shows a compression of approximately 35 in the xenon layer. If the line of sight was not exactly side on, the true compression would be higher. One-dimensional (1D) and 2D simulations discussed in the following provide further support of the creation of a radiatively collapsed shock.

IV. SIMULATION RESULTS

One can gain further insight into the impact of radiation on the experiment through simulations. We first discuss the results of simulations of this system using the 1D, Lagrangian, single-fluid-three-temperature code HYADES,[27] run using multigroup, diffusive radiation transport with 90 photon groups, adjusted to resolve the edges in the xenon opacity at up to 6 keV. The equation of state of xenon was the SESAME table.[28] In the regime of this experiment, the polytropic index (γ) inferred from the table is in the range of 1.2–1.3, as is appropriate for an ionizing medium that is dense enough that collisional recombination is dominant.[23] It is worth noting that the effective γ of xenon can be significantly smaller, e.g., in lower-density media in (more or less) coronal equilibrium, which is the case for the experiments with blast waves in gases.[22,29] The xenon was modeled using an average-atom, local-thermodynamic-equilibrium (LTE) description. One would expect this description and the radiation transport model to be qualitatively accurate but not fully predictive. As has been thoroughly documented through 2D simulations,[30] the laser irradiance used in such 1D simulations must be reduced to give accurate results, because radial heat transport reduces the ablation pressure in the actual system. Here it was adjusted to the level required to match the behavior of relevant purely hydrodynamic experiments.

The solid curve in Fig. 4(a) shows the above-mentioned radiative simulation results, whereas the dashed curve shows results of a simulation in which radiation is artificially suppressed. The shock transition is the right-most increase in density, which is moving to the right into preheated matter. The shocked xenon layer is just to the left of the shock tran-

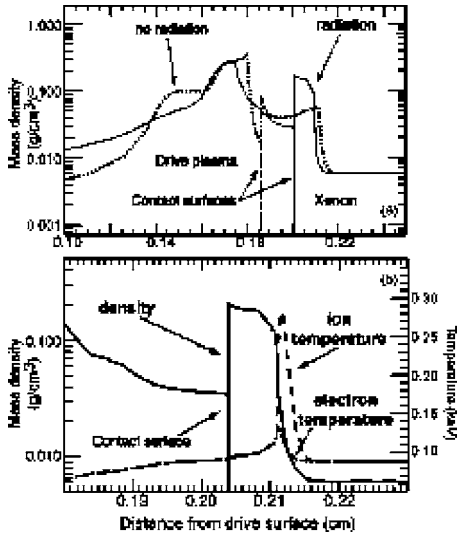

FIG. 4. (a) Density vs position from two Hyades simulations, at 16 ns, for experiments at a laser intensity of 10^{15} W/cm^2. The boundaries between the drive plasma, in this case Be, and the xenon are shown, labeled "contact surfaces." The solid line shows the result for multigroup, diffusive radiation transport, whereas the dashed line shows the result for a nonradiative system. When radiation is suppressed (dashed line), a collapsed layer does not form. (b) Density and temperature vs position from the Hyades simulation with radiation transport at 16 ns. The solid line is mass density, the dashed line is ion temperature, and the dash-dotted line is electron temperature. Note the difference in scales between (a) and (b).

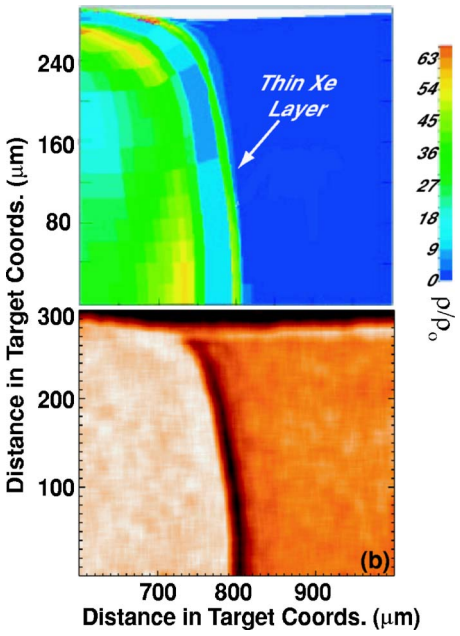

FIG. 5. (Color online) (a) Density profile at 7 ns, from a 2D simulation of the experiment, using the FCI code. The shock is moving to the right. The color bar calibrates the density as a ratio to the initial gas density. (b) Simulated radiograph, using density data from (a). Poisson noise and a point-spread function from data are included.

sition. In the radiative case one can see the postshock density increase due to cooling. This density increase is well resolved in this Lagrangian calculation, and shows a maximum compression of a factor of 35 over the initial gas density, compared to a maximum compression of 13 in the radiation-suppressed case. To the left of the contact surface is a more-structured layer of low-Z material. The structure in this layer has been established during the laser pulse, when there is shock reverberation in the driving material. The radiation has two effects. First, it narrows the shocked xenon layer by increasing its density. This is the primary effect one can detect using radiography. Second, it heats the low-Z material that is driving the shock and causes the xenon layer to separate from it. As the xenon layer radiates, radiation-driven ablation creates a distinct, low-density region between the dense driver material and the dense collapsed layer.[31] In Fig. 4(b) one can see the effects of radiative heating ahead of the shock, of the cooling that accompanies the density increase in the cooling layer, and of the radiative heating and ablation of the beryllium.

We also ran 2D simulations using the code FCI,[32,33] a Lagrangian, one-fluid, three-temperature code with multigroup diffusive radiation transport, an average atom non-LTE treatment of materials, and flux-limited electron heat transport. Figure 5(a) shows the calculated profile of mass density at 7 ns for a case with a 600 μm gas cell and an 820 μm laser spot. The density in most of the shocked layer is about 45 times the initial density, and there has been very little radial flow of mass out of the shocked layer. In the 2D simulations, the decrease of temperature ahead of the shock is more rapid than in 1D simulations, as one would expect due to the inclusion of radial radiation losses. Again, the low-Z material behind the shock is heated, and has separated from the xenon layer. This separation is clearly seen in Fig. 5(a), but not in radiography, because of the low absorption of the diagnostic x rays by low-Z material.

Figure 5(b) is a simulated radiograph based on the density profile shown in Fig. 5(a) and the experimental resolution. The boundary between xenon and beryllium is at the left edge of the right-most dense feature, whereas the dense feature at the top of the image is the plastic wall. Mass absorption coefficients for beryllium and xenon at 5.4 keV were taken from the National Institute for Standards and Technology FFAST database.[34] The source-induced broadening is 250 μm at the microchannel plate. Poisson noise estimated from representative experimental data is included, and the image is smoothed based on the instrumental smoothing determined from grid edges in data. This assumes also that the shock is observed from exactly side-on; if the shock were tilted by 5° from edge-on, a 50 μm thick, 600 μm diameter layer would appear almost 90 μm thick. Therefore, this method of detection gives an upper limit on the actual thickness of the layer, and thereby the density of the collapsed material.

V. CONCLUSIONS AND FUTURE DIRECTIONS

The layer of xenon produced by a nonradiative shock, with an effective γ of 1.2-1.3, would be from 140 to 220 μm thick at the location seen in Fig. 4, and the observed layer is 45 μm. Thus, one might suggest that the density has increased another factor of 3–4 in consequence of radiative losses, reaching a total of ~40 times the initial xenon density. The inferred density increase would be reduced to whatever extent material has left the shocked region by flowing

radially, although the 2D simulations find this to be small. However, this line-of-sight measurement will have a strong tendency to overestimate the thickness of the shocked layer, due to any tilt, curvature, or rippling of the shock front. A perfectly aligned measurement of the density profile shown in Fig. 3(a), with the resolution of the pinhole used, would produce a layer from 30 to 40 μm thick. Thus, it appears reasonable to conclude that we have observed a thin layer of shocked xenon whose density has been increased significantly by radiative losses.

Future experiments can work in several worthwhile directions. They can examine the structure of the shocked layer in more detail, can assess how it scales with parameters such as shock velocity and initial gas density, and can attempt to devise diagnostic approaches that can directly measure the properties of the shocked layer. In addition, by watching the long-term evolution of the shocked layer, such experiments might observe the onset of hydrodynamic instabilities like those discussed by Vishniac and Ryu.[35] Beyond such work, this system could be developed as a radiation source for experiments to examine other issues such as radiation transport.

ACKNOWLEDGMENTS

The authors acknowledge the vital contributions of the Omega technical staff, the target fabrication staff at Lawrence Livermore National Laboratory, Erika Roesler, Rebecca Gabl, and Peter Susalla, as well as for useful discussions with Dmitri Ryutov and Russell Wallace.

This work is supported by the National Nuclear Security Agency under DOE Grant Nos. DE-FG03-99DP00284 and DE-FG03-00SF22021, and by other grants and contracts.

[1] R. P. Drake, *High Energy Density Physics: Foundations of Inertial Fusion and Experimental Astrophysics* (Springer, New York, 2006).
[2] D. Mihalas and B. Weibel-Mihalas, *Foundations of Radiation Hydrodynamics* (Dover, Mineola, NY, 1999).
[3] F. H. Shu, *The Physics of Astrophysics: Gas Dynamics* (University Science Books, Mill Valley, CA, 1992).
[4] R. P. Drake, Astrophys. Space Sci. **298**, 49 (2005).
[5] L. Ensman and A. Burrows, Astrophys. J. **393**, 742 (1992).
[6] N. Calvet and E. Gullbring, Astrophys. J. **509**, 802 (1998).
[7] A. Hujeirat and J. C. B. Papaloizou, Astron. Astrophys. **340**, 593 (1998).
[8] S. A. Lamzin, Astrophys. Space Sci. **261**, 137 (1999).
[9] R. A. Chevalier and C. Fransson, Astrophys. J. **420**, 268 (1994).
[10] K. J. Borkowski, J. M. Blondin, and R. McCray, Astrophys. J. **477**, 281 (1997).
[11] K. J. Borkowski, J. M. Blondin, and R. McCray, Astrophys. J. Lett. **476**, 31 (1997).
[12] B. Reipurth and J. Bally, Annu. Rev. Astron. Astrophys. **39**, 403 (2001).
[13] J. M. Blondin, E. B. Wright, K. J. Borkowski *et al.*, Astrophys. J. **500**, 342 (1998).
[14] M. J. Edwards, A. J. MacKinnon, J. Zweiback *et al.*, Phys. Rev. Lett. **87**, 0850041 (2001).
[15] P. A. Keiter, R. P. Drake, T. S. Perry *et al.*, Phys. Rev. Lett. **89**, 165003 (2002).
[16] J. C. Bozier, G. Thiell, J. P. Le-Breton *et al.*, Phys. Rev. Lett. **57**, 1304 (1986).
[17] J. Grun, J. Stamper, C. Manka *et al.*, Phys. Rev. Lett. **66**, 2738 (1991).
[18] S. Bouquet, C. Stéhlé, M. Koenig *et al.*, Phys. Rev. Lett. **92**, 225001 (2004).
[19] M. Koenig, A. Benuzzi-Mounaix, N. Grandjouan *et al.*, Shock Compression of Condensed Matter-2001 (2001), p. 1367.
[20] M. Koenig, T. Vinci, A. Benuzzi-Mounaix *et al.*, Astrophys. Space Sci. **298**, 69 (2005).
[21] T. Vinci, Phys. Plasmas **13**, 010702 (2006).
[22] J. M. Laming and J. Grun, Phys. Rev. Lett. **89**, 125002 (2002).
[23] R. P. Drake and A. B. Reighard, AIP Conf. Proc. **1**, 1417 (2006).
[24] K. S. Budil, D. M. Gold, K. G. Estabrook *et al.*, Astrophys. J., Suppl. Ser. **127**, 261 (2000).
[25] L. M. Barker and J. Hollenback, J. Appl. Phys. **43**, 1669 (1972).
[26] A. B. Reighard, R. P. Drake, K. K. Dannenberg *et al.*, in *Proceedings of Inertial Fusion Science and Applications Conference* (American Nuclear Society, Inc., Monterey, CA, 2003), Vol. 1, p. 950.
[27] J. T. Larsen and S. M. Lane, J. Quant. Spectrosc. Radiat. Transf. **51**, 179 (1994).
[28] SESAME: The Los Alamos National Laboratory Equation of State Database, LA-UR-92–3407 (1992).
[29] E. Liang and K. Keilty, Astrophys. J. **533**, 890 (2000).
[30] D. G. Braun (private communication).
[31] M. Herrmann (private communication).
[32] R. Dautray and J.-P. Watteau, *La Fusion Thermonucleaire par Laser* (Eyrolles, Paris, 1993).
[33] G. Schurtz, in *La Fusion Thermonucleaire Inertielle par Laser*, edited by R. Dautray (Eyrolles, Paris, France, 1994), Vol. 2, p. 1055.
[34] C. T. Chantler, K. Olsen, R. A. Dragoset *et al.* (National Institute of Standards and Technology, 2005).
[35] E. T. Vishniac and D. Ryu, Astrophys. J. **337**, 917 (1989).